BIOCHEMISTRY
including biophysical chemistry & molecular biology

Article

pubs.acs.org/biochemistry

The C-Terminal Threonine of Aβ43 Nucleates Toxic Aggregation via Structural and Dynamical Changes in Monomers and Protofibrils

Alexander E. Conicella[†] and Nicolas L. Fawzi*[,‡]

[†]Graduate Program in Molecular Biology, Cell Biology, and Biochemistry and [‡]Department of Molecular Pharmacology, Physiology, and Biotechnology, Brown University, Providence, Rhode Island 02912, United States

Supporting Information

ABSTRACT: Recent studies suggest that deposition of amyloid β (Aβ) into oligomeric aggregates and fibrils, hallmarks of Alzheimer's disease, may be initiated by the aggregation of Aβ species other than the well-studied 40- and 42-residue forms, Aβ40 and Aβ42, respectively. Here we report on key structural, dynamic, and aggregation kinetic parameters of Aβ43, extended by a single threonine at the C-terminus relative to Aβ42. Using aggregation time course experiments, electron microscopy, and a combination of nuclear magnetic resonance measurements including backbone relaxation, dark-state exchange saturation transfer, and quantification of chemical shift differences and scalar coupling constants, we demonstrate that the C-terminal threonine in Aβ43 increases the rate and extent of protofibril aggregation and confers slow C-terminal motions in the monomeric and protofibril-bound forms of Aβ43. Relative to the neighboring residues, the hydrophilic Thr43 of Aβ43 favors direct contact with the protofibril surface more so than the C-terminus of Aβ40 or Aβ42. Taken together, these results demonstrate the potential of a small chemical modification to affect the properties of Aβ structure and aggregation, providing a mechanism for the potential role of Aβ43 as a primary nucleator of Aβ aggregates in Alzheimer's disease.

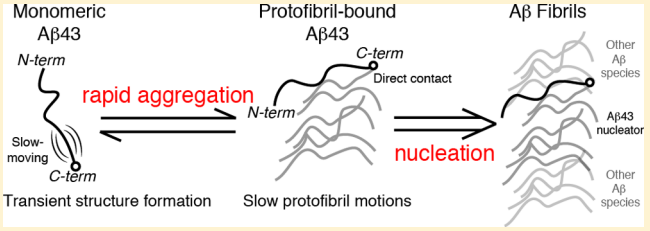

The triggers for the aberrant formation of extracellular plaques of the amyloid β (Aβ) peptide and intracellular neurofibrillary tangles of the protein tau remain as critical unanswered questions in Alzheimer's disease (AD) research. Although the amyloid cascade hypothesis posits that the aggregation-prone Aβ peptides are the causative agents in AD,[1] deposition of Aβ into the ordered amyloid fibrils that are the primary component of plaques correlates only weakly with disease severity.[2] Subsequent studies have suggested therefore that the primary toxic species in AD are lower-molecular weight aggregates of Aβ lacking the highly organized structure of amyloid fibrils.[3] Supporting this hypothesis, numerous studies have demonstrated that soluble Aβ aggregates, including both oligomers (aggregates consisting of 2−20 peptides) and protofibrils (intermediates on the amyloid fibril formation pathway consisting of hundreds of peptides), are neurotoxic in cell culture and their presence correlates with the progression of AD.[4,5] Definitive proof of the "toxic oligomer" hypothesis has yet to emerge, however, hampered by a critical lack of clarity regarding the mechanism of neuronal toxicity and the structures of the diverse array of nonfibrillar assemblies of Aβ formed *in vivo* and even *in vitro*,[6] motivating efforts to characterize the structural details of the assembly process.

Formed by progressive proteolytic cleavage of the amyloid precursor protein (APP), Aβ peptides are found in lengths ranging from 39 to 49 amino acids.[7] Aβ40 and Aβ42 are the primary products of the stepwise cleavage by γ-secretase of the C99 C-terminal fragment of APP along two lineages: Aβ49 → Aβ46 → Aβ43 → Aβ40 → Aβ38/37 and Aβ48 → Aβ45 → Aβ42 → Aβ39.[8] Aβ40, the most abundant, 40-amino acid form, is significantly less prone to aggregation than Aβ42, the 42-amino acid form extended at the C-terminus by two hydrophobic residues, isoleucine and alanine.[9] Mutations in APP that result in higher ratios of Aβ42 to Aβ40 cause familial Alzheimer's disease (FAD), underscoring the connection between the aggregation propensity of the C-terminal region of Aβ and the occurrence of AD.[10] Although Aβ peptides are primarily unstructured as monomers, NMR experiments probing backbone and side chain dynamics have demonstrated that Aβ42 has a more rigid C-terminal region compared to that of Aβ40,[11−13] suggesting that slower motions in this region contribute to the enhanced aggregation propensity of Aβ42. Recent technical advances have made it possible to characterize the structure of both fibrillar[14−16] and nonfibrillar (oligomeric and protofibrillar) aggregates[17−24] of Aβ and their interactions with monomeric Aβ[25] with atomistic resolution despite the challenges associated with the large size, disordered structure, and transient nature of aggregates. Using dark-state exchange saturation transfer (DEST) NMR to probe the atomic-resolution structure and dynamics of peptides within cytotoxic Aβ protofibrillar aggregates ranging from 2 to 20 MDa lacking the linear, unbranched ordered structure of mature amyloid fibrils, we have recently demonstrated that the two additional

Received: January 30, 2014
Revised: April 25, 2014
Published: April 28, 2014

residues in Aβ42 significantly slow motions across the entire C-terminal region of Aβ42 (residues 31−42) in the protofibril-bound state, suggesting that slowed motions may contribute to aggregation propensity.[26]

Although the toxicity of oligomeric forms of Aβ and their presence in disease are well-established, the trigger for the formation of toxic oligomers from the constitutively present Aβ peptides is unknown. Recently, several studies have demonstrated that other Aβ variants, including N-terminally truncated pyroglutamate-modified Aβ (e.g., pE3-42) and extended C-terminal forms (e.g., Aβ43), may be more prone to aggregation than Aβ42 and may play a critical role in AD by nucleating Aβ aggregation.[27,28] Bearing a single additional threonine at the C-terminus relative to Aβ42, Aβ43 appears more frequently in AD amyloid plaques than Aβ40[29] despite a 1000-fold lower cortical concentration.[30] Aβ43 is enriched 20- and 40-fold in the frontal and occipital cortices, respectively, of patients with sporadic AD compared to nondiseased controls, twice the enrichment of Aβ42 and 1 order of magnitude more enriched than Aβ40.[30] In a transgenic APP-expressing mouse model of AD, Aβ43 is the earliest depositing Aβ species, suggesting Aβ43 plays a crucial role in the early stages of AD progression as a nucleator of Aβ aggregates.[31] Previous studies have demonstrated that Aβ43 has aggregation properties similar to those of Aβ42,[28,32] yet Aβ43 is significantly more neurotoxic when applied to cells in culture.[28] Furthermore, earlier onset of memory impairment, neuropathology, and plaque formation is observed in a mouse model of AD in which a knock-in γ-secretase bearing an FAD mutation increases the level of Aβ43 production without changing Aβ42 levels.[28]

Given the demonstrated potential of Aβ43 to be a nucleator of toxic aggregates in AD, several important open questions remain regarding the biophysical chemistry of Aβ43. Is Aβ43 more prone to forming toxic aggregates than Aβ42? If so, why does the addition of a hydrophilic amino acid at the C-terminus of Aβ lead to greater aggregation propensity typically associated with hydrophobically driven self-association? A clear understanding of the biophysical properties of Aβ43 and its aggregates will provide insight into its involvement in AD and serve as critical data for a potential target for future AD therapeutics. In this study, we characterize the monomeric and protofibril-bound states of Aβ43 under conditions that stabilize protofibrils using solution NMR experiments sensitive to both the structure and motions of Aβ peptides, properties that are known to distinguish the aggregation propensity of shorter Aβ variants. By demonstrating that the additional C-terminal threonine speeds and enhances protofibril formation, alters the C-terminal monomer structural ensemble, and contributes to slower motions of the peptide in both the monomeric and protofibril-bound states, we provide a detailed characterization of the aggregation and structural properties of Aβ43 that contribute to its unique role in AD.

MATERIALS AND METHODS

Preparation of Aβ Samples. Uniformly ^{15}N-labeled Aβ43, Aβ42, and Aβ40 were purchased from rPeptide (Bogart, GA). To remove preformed aggregates, samples were prepared from NaOH-treated lyophilized stocks as described previously.[26] Aβ43 samples were diluted to concentrations of 120, 25, and 15 μM in 50 mM HEPES (pH 6.8) and a 90% H_2O/10% D_2O mixture and maintained at 10 °C at all times unless otherwise noted. Protofibril formation of 120 μM Aβ43 was monitored using a time course of ^{1}H−^{15}N heteronuclear single-quantum coherence (HSQC) correlation spectra cross peak intensities. Establishment of an equilibrium between monomers and protofibrils (i.e., <10% change per day in the concentration of monomers as measured by monomer resonance intensities) in 120 μM Aβ43 samples occurred between 24 and 48 h, and NMR experiments characterizing monomer−protofibril interaction were performed after this point. For characterization of transverse relaxation rates and scalar coupling constants of monomeric Aβ peptides, 25 μM Aβ42 and 50 μM Aβ40 were prepared as described above. Measurements of ^{1}H−^{13}C HSQC at natural abundance ^{13}C were taken in 20 mM sodium phosphate (pH 6.8) to prevent ^{13}C signals arising from HEPES buffer.

To investigate the effects of secondary structure on Aβ chemical shifts and R_2 values, we prepared lyophilized stocks of ^{15}N-labeled Aβ43 and Aβ42 as described above and diluted them to 100 μM in 7.2 M urea, 50 mM HEPES (pH 6.9), and a 95% H_2O/5% D_2O mixture.

Electron Microscopy. Aliquots for transmission electron microscopy (TEM) studies were taken from 120 μM Aβ43 NMR samples and diluted to 165 nM with 50 mM HEPES (pH 6.8) and a 90% H_2O/10% D_2O mixture. Four microliters of the diluted Aβ43 solution was immediately spotted onto an ultrathin carbon film on holey carbon support grids (product code 01824, Ted Pella, Reading, CA), washed three times with deionized H_2O, stained with 5 μL of 3% uranyl acetate (Electron Microscopy Sciences, Hatfield, PA) for 60 s, blotted, and left to air-dry. TEM sample grids were then imaged with a Philips 410 transmission electron microscope.

Solution NMR Experiments. All NMR experiments were recorded at 10 °C using a Bruker Avance III HD NMR spectrometer operating at a ^{1}H frequency of 850 MHz equipped with a Bruker TCI *z*-axis gradient cryogenic probe. Experimental sweep widths and acquisition times (i.e., resolution) and the number of transients were optimized for the necessary resolution, experiment time, and signal-to-noise ratio for each experiment type but kept constant for the same experiment conducted with different peptide (i.e., Aβ40, Aβ42, and Aβ43) samples and different concentration conditions.

To measure the difference in transverse relaxation rates in the presence and absence of Aβ43 protofibrils, in-phase ^{15}N transverse relaxation rates (^{15}N R_2) were measured for Aβ43 at 120 and 25 μM with an interleaved Carr−Purcell−Meiboom−Gill (CPMG) experiment (hsqct2etf3gpsi3d, Topspin version 3.2, Bruker). Each interleaved experiment comprises 90* and 1360* complex data pairs in the indirect ^{15}N and direct ^{1}H dimensions, respectively, with corresponding acquisition times of 66 and 160 ms and sweep widths of 15.8 and 10 ppm centered at 119 and 4.9 ppm, respectively. A CPMG field of 556 Hz was used for all transverse relaxation measurements with total R_2 relaxation CMPG loop lengths of 16.4, 32.9, 65.7, 131.4, 197.2, and 295.7 ms. An interscan delay of 2.5 s was used. Data were processed with nmrPipe[33] as follows. Data were apodized with a 10 Hz Gaussian function for the ^{1}H dimension and a cosine bell function for the ^{15}N dimension. To resolve peaks for residues D7 and D23 only, spectra were additionally processed separately with the following change: free induction decays were apodized with a 2 Hz exponential line broadening for the ^{1}H dimension. Best-fit R_2 relaxation rates were calculated by least-squares optimization of ^{1}H/^{15}N peak intensities to single-exponential decay functions. Given the low NMR signal intensity due to only ∼12 μM Aβ43 remaining monomeric at a total concentration of 120 μM,

independent measurements of R_2 were recorded, and the resulting transverse relaxation rates were averaged. ΔR_2, the difference in ^{15}N R_2 values in the presence (120 μM) and absence (25 μM) of protofibrils, was then calculated.

Dynamical differences in monomeric (15 and 25 μM samples) Aβ42 and Aβ43 were observed by measurement of ^{15}N R_1, temperature-compensated ^{15}N R_2, and heteronuclear NOE experiments using standard pulse sequences (hsqct1etf3gpsi3d, hsqct2etf3gpsitc3d, and hsqcnoef3gpsi, respectively, from Topspin version 3.2). Each R_2 experiment comprised six interleaved CPMG ^{15}N R_2 relaxation times of 16.4, 49.3, 82.2, 131.4, 197.2, and 263.7 ms at a CPMG field strength of 556 Hz. Each interleaved two-dimensional experiment comprised 128* and 1360* complex data points in the indirect ^{15}N and direct ^{1}H dimensions, respectively, with corresponding acquisition times of 94 and 160 ms and sweep widths of 15.8 and 10 ppm centered at 119 and 4.9 ppm, respectively. Experiments were conducted with 16 transients per free induction decay and an interscan delay of 2.5 s, resulting in a total experiment time of 2 days. Data were processed as described above. Each R_1 experiment comprised seven interleaved ^{15}N R_1 relaxation times of 100, 200, 300, 400, 600, 800, and 1000 ms, with acquisition and processing parameters identical to those described for R_2. Heteronuclear NOE experiments were conducted with a 5 s interscan delay (>5T_1 as measured), interleaving FIDs with and without saturation, and 48 transients per free induction decay, with acquisition and processing parameters identical to those described for R_2.

To determine if differences in chemical shift and R_2 observed for Aβ43 and Aβ42 arise due to structural changes, $^{1}H-^{15}N$ HSQC spectra and temperature-compensated ^{15}N R_2 experiments were measured for 100 μM Aβ43 and Aβ42 in 7.2 M urea, as described above. Each R_2 experiment comprised six interleaved CPMG ^{15}N R_2 relaxation time points of 16.4, 49.3, 82.2, 131.4, 197.2, and 263.7 ms at a CPMG field strength of 556 Hz. Each interleaved two-dimensional experiment comprises 128* and 1360* complex data points in the indirect ^{15}N and direct ^{1}H dimensions, respectively, with corresponding acquisition times of 74 and 160 ms and sweep widths of 20 and 10 ppm centered at 117.75 and 4.9 ppm, respectively. Experiments were conducted with four transients per free induction decay and an interscan delay of 2.5 s, resulting in a total experiment time of 5.5 h. Data were processed as described above.

Probing of the protofibril-bound state of Aβ43 present at 120 μM was accomplished with dark-state exchange saturation transfer (DEST) NMR spectroscopy using a series of interleaved, HSQC-based experiments.[26,34] Briefly, initial ^{1}H magnetization is transferred to $^{15}N_z$ by a refocused INEPT element, preferentially saturated in the protofibril-bound state by 400 ms ^{15}N radiofrequency (RF) continuous wave pulses applied at a power of 500 or 375 Hz and ^{15}N carrier frequency offsets between 6 and −6 kHz (for 500 Hz, 6, 4, 2.5, −2.5, −4, and −6 kHz offsets; for 375 Hz, 4, 2.5, and −2.5 kHz offsets; three reference experiments with no applied RF field), transferred to the NMR-visible monomeric species by chemical exchange, and detected after INEPT transfer to ^{1}H. Each interleaved two-dimensional experiment comprises 90* and 2048* complex data points in the indirect ^{15}N and direct ^{1}H dimensions, respectively, with corresponding acquisition times of 66 and 229 ms and sweep widths of 15.8 and 10.5 ppm centered around 119 and 4.9 ppm, respectively. Data were processed as described above. Attenuation of the NMR signal due to dark-state exchange saturation transfer of each resonance was normalized to the average intensity of each resonance in the three interleaved reference experiments (with no RF power).

Quantification of Spectral Differences between Monomeric Aβ42 and Aβ43. Chemical shift differences between Aβ42 and Aβ43 monomers were obtained from $^{1}H-^{15}N$ HSQC experiments measured at 10 and 37 °C. Each experiment comprised 64* and 2048* complex data points in the indirect ^{15}N and direct ^{1}H dimensions, respectively, with corresponding acquisition times of 31 and 229 ms and sweep widths of 24 and 10.5 ppm centered at 119 and 4.9 ppm (4.7 ppm at 37 °C), respectively. Experiments were conducted with eight transients per free induction decay. Data were processed as described above. To resolve the overlap for residues D7, A21, V24, I31, I32, and M35, direct ^{1}H dimension data were separately processed with 1 Hz exponential line broadening.

$^{1}H-^{13}C$ HSQC experiments conducted at 10 °C comprised 256* and 1024* complex data points in the ^{13}C and direct ^{1}H dimensions, respectively, with 96 transients per free induction decay. Data were processed as described above.

For 100 μM Aβ43 and Aβ42 samples prepared in 7.2 M urea, chemical shift differences were quantified from similar $^{1}H-^{15}N$ HSQC experiments. Each experiment comprised 128* and 2048* complex data points in the indirect ^{15}N and direct ^{1}H dimensions, respectively, with corresponding acquisition times of 62 and 229 ms and sweep widths of 24 and 10.5 ppm centered at 119 and 4.9 ppm, respectively. Experiments were conducted with two transients per free induction decay. Data were processed as described above, with 6.5 Hz Gaussian line broadening in the direct ^{1}H dimension.

$^{3}J_{HN\text{-}H\alpha}$ scalar coupling constants for 50 μM Aβ40, 25 μM Aβ42, and 25 μM Aβ43 were obtained from alternate processing of the high-signal-to-noise ratio HSQC experiment derived from a ^{15}N R_2 relaxation time point (16.4 ms) of the temperature-compensated ^{15}N R_2 experiments (see above) for 10 °C values, and from HSQC spectra (see above) for 37 °C values. Free induction decays were apodized with 1 Hz exponential line broadening in the direct ^{1}H dimension, and a cosine bell function in the indirect ^{15}N dimension. $^{3}J_{HN\text{-}H\alpha}$ values were determined by line-shape analysis using a custom script in the software program R where the center position, widths, and intensities of two Lorentzian functions were best fit to the ^{1}H dimension slices for the resonances corresponding to each backbone $^{1}H-^{15}N$ pair.

DEST Model Fitting. Kinetic and dynamic parameters describing Aβ43 monomer−protofibril interactions and the Aβ43 protofibril-bound state were derived from experimental NMR data with DESTfit as previously described.[34] Briefly, DESTfit was run with a pseudo-two-state fit type with the apparent first-order association rate constant (k_{on}^{app}) set to the maximal observed ΔR_2, as previously conducted in the analysis of DEST data for Aβ40 and Aβ42.[26,34]

RESULTS

Aβ43 Assembles into Protofibrils Faster and to a Greater Extent Than Aβ42 or Aβ40. To determine the *in vitro* aggregation properties of Aβ43, $^{1}H-^{15}N$ HSQC peak intensities of resolved resonances (Figure 1) were monitored as a function of time for ^{15}N-labeled Aβ43 (120 and 25 μM). At low concentrations (25 μM), Aβ43 aggregation is minimal and Aβ43 remains ≈95% monomeric after 2 days. However, at a

dx.doi.org/10.1021/bi500131a | *Biochemistry* 2014, 53, 3095−3105

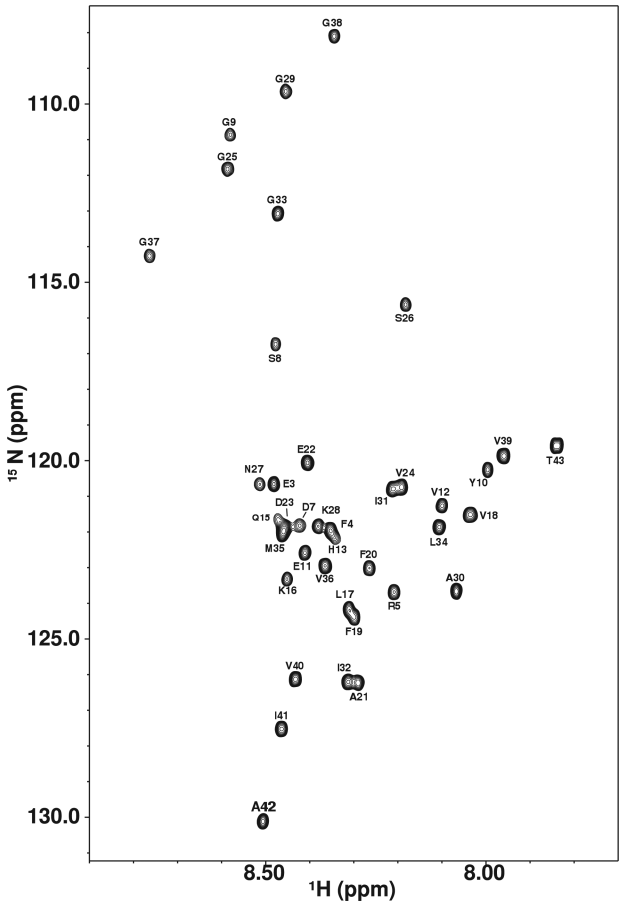

Figure 1. Backbone amide region of $^{1}H-^{15}N$ heteronuclear single-quantum coherence (HSQC) spectrum of 25 μM Aβ43.

higher concentration (120 μM), Aβ43 aggregates rapidly with the intensity of NMR signals decreasing to ~10% of the original value within 1 day (Figure 2a). Transmission electron microscopy analysis of 120 μM Aβ43 over time confirms that the loss of the monomeric Aβ43 signal intensity is concomitant with the formation of protofibrils. Protofibrils can be detected as little as 1 h after sample creation and are present at a much higher concentration after 24 h (Figure 2b,c). Although the atomic level structure and the heterogeneity of the contacts stabilizing the core of protofibrils formed by each Aβ variant are unknown, Aβ43 protofibrils are morphologically similar as determined by microscopy to those we have previously observed for Aβ42 and Aβ40.[26] The rate of aggregation can be described by fitting $^{1}H-^{15}N$ HSQC peak intensities to the exponential decay function $I(t)/I_0 = (1 - A_1)e^{-t/\tau_1} + A_1$, where τ_1 is a time constant for protofibril formation and A_1 is a constant representing the fraction remaining monomeric after protofibril formation reaches equilibrium. Best-fit parameters for Aβ43 protofibril formation under these conditions are as follows: $\tau_1 = 6 \pm 1$ h, and $A_1 = 10 \pm 4\%$. This aggregation is much more rapid than for Aβ40 or Aβ42, each of which requires >1 week to complete protofibril formation under identical conditions.[8] Protofibril formation also proceeds to a greater extent for Aβ43. After protofibril formation for 2 weeks, only 12 μM peptide remains monomeric compared to 20 μM Aβ42 or 120 μM Aβ40 at similar concentrations.[26] Therefore, the addition of T43 both accelerates, and decreases the critical concentration for, Aβ protofibril formation. At 37 °C, samples at concentrations of 25 μM that are stable at 10 °C rapidly

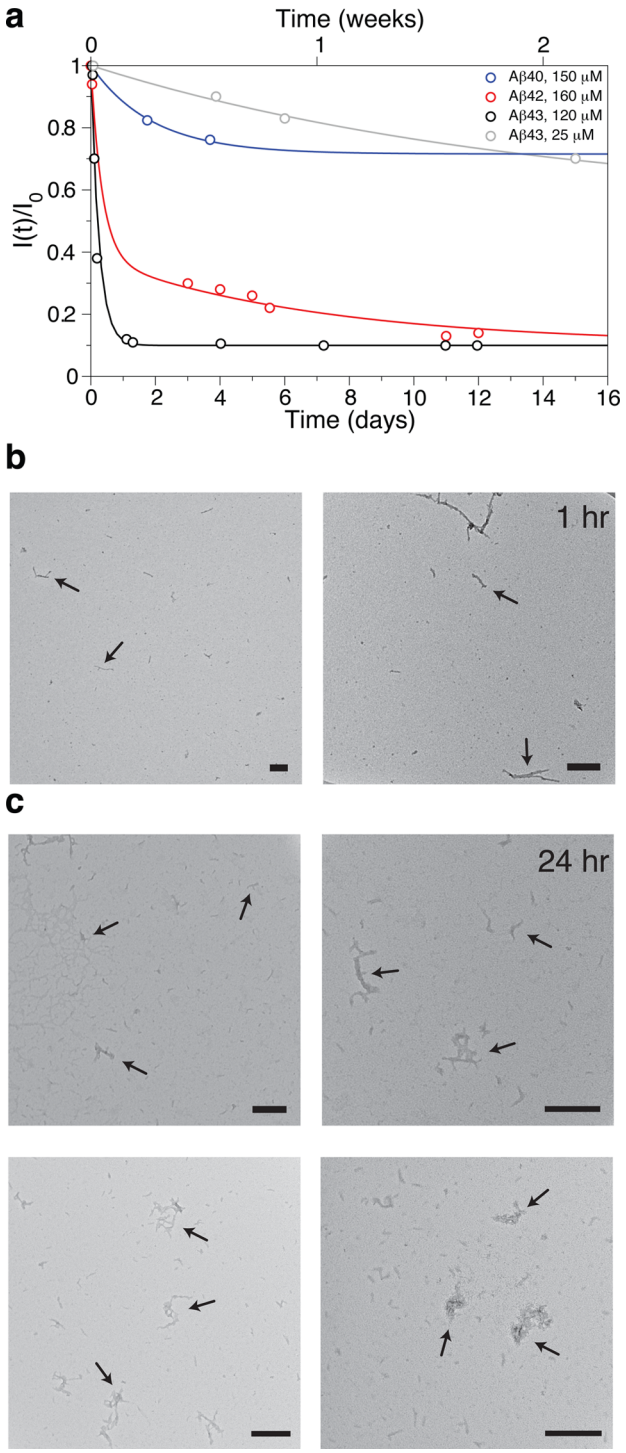

Figure 2. Aβ43 aggregates into protofibrillar species in a concentration-dependent and time-dependent manner. (a) The ratio of monomeric NMR signal intensity $[I(t)/I_0]$ decays exponentially as a function of time. Aβ43 at concentrations of 25 μM (gray) and 120 μM (black) was monitored via HSQC cross peak intensities for over 2 weeks. The significantly slower aggregation of similar concentrations of Aβ42 (160 μM, red) and Aβ40 (150 μM, blue) under identical conditions is shown for comparison (data for Aβ40 and Aβ42 from ref 26). Transmission electron microscopy images of 120 μM Aβ43 showing that (b) protofibrils are visible as little as 1 h after sample preparation and (c) protofibrils are present at a higher concentration after 24 h. Arrows highlight some of the protofibrils present, although many more are evident within each image. Scale bars represent 200 nm.

dx.doi.org/10.1021/bi500131a | *Biochemistry* 2014, 53, 3095−3105

aggregate (Figure S1 of the Supporting Information) into micrometer length fibrillar structures much larger than the protofibrils formed at higher concentrations at 10 °C, consistent with observations that low-temperature conditions stabilize not only the monomer but also the protofibrillar intermediates.[26] As observed for aggregation at 10 °C, faster rates of monomer signal decay are observed for Aβ43 (τ_1 = 0.45 ± 0.02 h, and A_1 = 12 ± 1%) than for Aβ42 (τ_1 = 0.94 ± 0.17 h, and A_1 = 23 ± 5%).

C-Terminal Motions of Aβ43 Monomers Slowed Compared to Those of Aβ42 Monomers. The following series of NMR experiments characterizing the structure and dynamics of the monomeric and protofibril-bound states of Aβ43 compared to Aβ42 (Figure 3) provides a rationale for

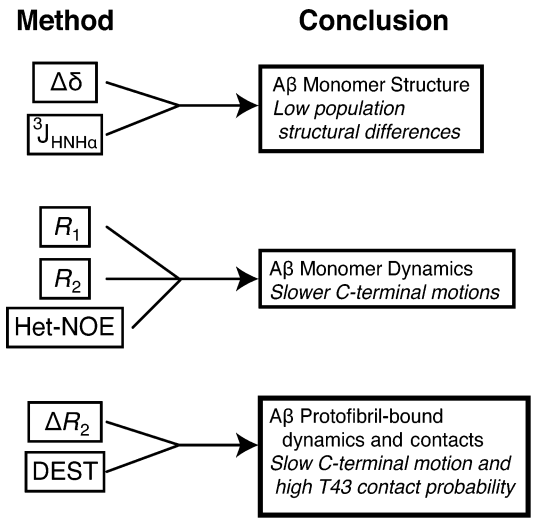

Figure 3. Diagram of the NMR experiments conducted, the phenomena probed by these experiments, and a summary of the results.

how the addition of T43 results in the observed differences in aggregation. Fast (picosecond to nanosecond) time scale motions of the backbone positions of monomeric Aβ43 were compared to those of Aβ42 to determine if slower peptide dynamics contribute to the increased aggregation propensity of Aβ43, as observed by Wang and co-workers for Aβ40 and Aβ42.[12] Therefore, we measured ^{15}N R_2, ^{15}N R_1, and heteronuclear NOE for both Aβ42 and Aβ43 under identical conditions. As expected for the hydrophilic N-terminal region (residues 3−10), no significant differences were observed between relaxation parameters for Aβ43 and Aβ42, showing that the N-terminal regions of Aβ behave the same regardless of C-terminal length. However, ^{15}N R_2 values for residues 17−42 in Aβ43, encompassing the entire central and C-terminal hydrophobic regions, are significantly higher than those for Aβ42 (Figure 4a), suggesting Aβ43 has slower motions than Aβ42 across the majority of the peptide. To confirm that the observed increases in R_2 values are not the result of interactions between Aβ43 monomers and spontaneously formed trace protofibrils potentially present at a concentration of 25 μM, R_2 values were measured for freshly prepared 15 μM Aβ43 where the concentration of any trace aggregates would be lower. Although the signal-to-noise ratio decreased and the uncertainty in R_2 increased, no systematic decrease in R_2 was observed for Aβ43 at 15 μM compared to Aβ43 at 25 μM (Figure S2 of the Supporting Information), indicating the

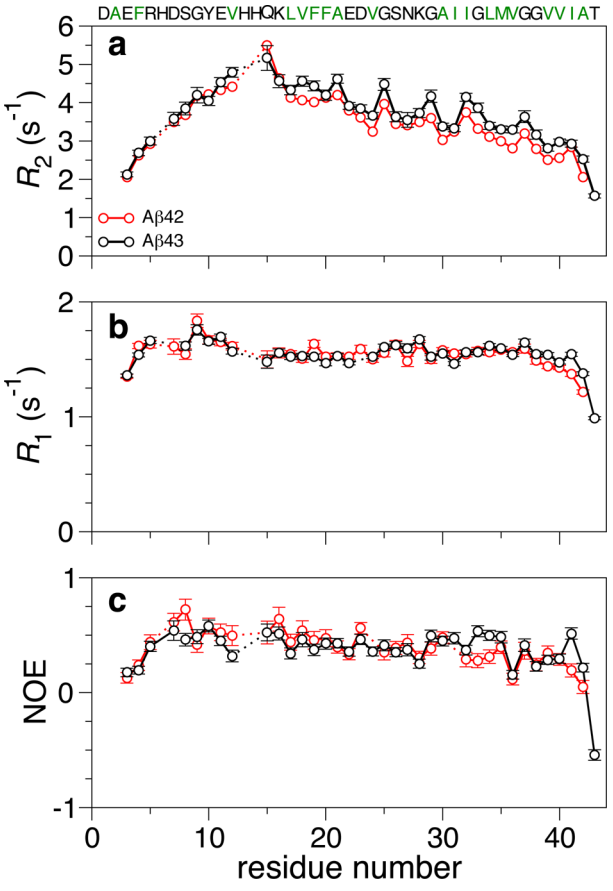

Figure 4. Dynamics of the backbone of monomeric Aβ42 and Aβ43 as measured by (a) ^{15}N R_2, (b) ^{15}N R_1, and (c) heteronuclear ^{15}N−{^{1}H} nuclear Overhauser effect (hetNOE) values. Dynamical differences on the picosecond to nanosecond time scale are observed for the central (R_2) and C-terminal regions (R_2, R_1, and hetNOE) of Aβ43. Error bars denote one standard deviation. Hydrophobic residues appear in green.

values at 25 μM Aβ43 faithfully represent those of the free Aβ43 monomer.

Furthermore, significantly higher values of the heteronuclear NOE, associated with slower motions, are observed at positions 34, 35, 41, and 42 in Aβ43 (Figure 4c). In addition, R_1 is significantly higher from residue 38 through the C-terminus in Aβ43 (Figure 4b) just as was previously observed in the more rigid C-terminus of Aβ42 compared to that of Aβ40.[12] A higher ^{15}N R_1 is expected for slower motions under these conditions and field because of the contribution of <1 ns time scale motion to backbone relaxation in a disordered peptide.[35] Together, ^{15}N backbone dynamics experiments confirm that dynamical differences, specifically slower motions, across the picosecond to nanosecond time scale are present in the C-terminal hydrophobic region of Aβ43 compared to that of Aβ42.

To determine whether the slower C-terminal motions observed for Aβ43 are a result of an increased propensity of Aβ43 to form stable structure or simply due to the higher molecular weight of Aβ43, we compared the ^{15}N R_2 values in native buffer to those under denaturing conditions [100 μM Aβ43 or Aβ42 in 7.2 M urea with the same buffer used previously, 50 mM HEPES (pH 6.9)] where any stable or transient secondary structure should be disrupted. Under denaturing conditions, the difference between ^{15}N R_2 values for Aβ42 and Aβ43 is nearly completely suppressed (Figure S3 of the Supporting Information), suggesting that slower dynamics

dx.doi.org/10.1021/bi500131a | Biochemistry 2014, 53, 3095−3105

observed across the central and C-terminal regions of Aβ43 under native conditions are due to the formation of transient structure.

Structural Changes in the C-Terminal Region of Monomeric Aβ Induced by T43. To interrogate changes in structure that give rise to the observed dynamical differences, we measured the chemical shift differences between monomeric Aβ43 and Aβ42. Chemical shifts are sensitive reporters of structure and structural changes that are especially useful in systems such as Aβ43 where a low sample concentration and a disordered structural ensemble preclude characterization by traditional (^{1}H−^{1}H NOE-based) NMR structural methods.[36] The differences between ^1H_N and ^{15}N chemical shift deviations ($\Delta\delta$) for Aβ43 and Aβ42 were measured under native conditions. Throughout the first 20 residues, absolute ^1H_N and ^{15}N chemical shift differences were small, not exceeding 0.003 and 0.02 ppm (Figure 5), respectively. However, large

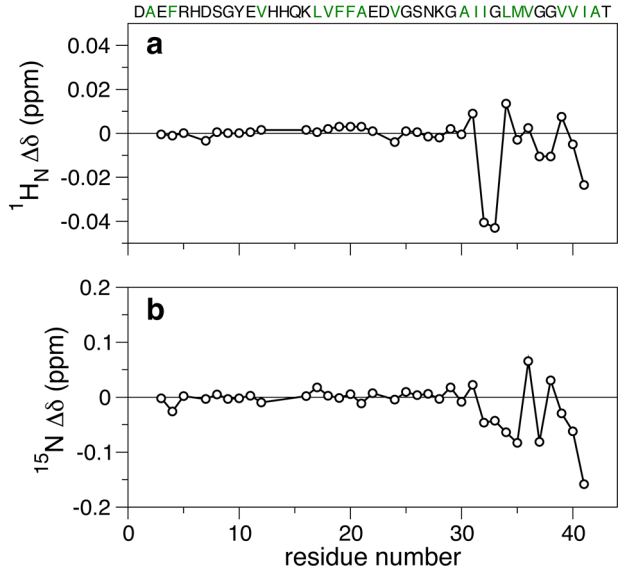

Figure 5. Chemical shift differences between monomeric Aβ42 and Aβ43 span from residue 31 to the C-terminus. Differences in (a) proton, ^1H_N $\Delta\delta$, and (b) nitrogen, ^{15}N $\Delta\delta$, chemical shifts between Aβ43 and Aβ42. Large changes in chemical shifts for residue A42 in Aβ42 and Aβ43 due to terminal effects are not shown.

differences were observed across the C-terminal region with ^1H_N and ^{15}N $\Delta\delta$ values for residues I32 and G33 exceeding −0.04 ppm. Given the long sequence distance between residues I32 and G33 and the Aβ43 C-terminus, the large $\Delta\delta$ values for these residues are unlikely to result from a peptide conformation-independent mechanism,[37] suggesting that the Aβ43 C-terminal structural ensemble is distinct from that of Aβ42. Further supporting this hypothesis that the chemical shift differences between Aβ43 and Aβ42 are caused by differences in the structural ensemble, C-terminal chemical shift differences between Aβ43 and Aβ42 are preserved at 37 °C and are decreased by a factor of approximately 2 under denaturing conditions (Figure S4 of the Supporting Information).

To investigate if differences in local secondary structure contribute to the ^1H_N chemical shift differences observed between Aβ43 and Aβ42, $^3J_{HN\text{-}H\alpha}$ coupling constants sensitive to backbone ϕ angles were obtained by line-shape analysis of high-resolution ^{1}H HSQC spectra. Our measured $^3J_{HN\text{-}H\alpha}$ couplings correlate extremely well with previously reported $^3J_{HN\text{-}H\alpha}$ values for Aβ40 and Aβ42 (Figure S5 of the Supporting Information)[38] and are similar for Aβ40, Aβ42, and Aβ43 throughout the majority of the peptide (residues E3−V39). However, $^3J_{HN\text{-}H\alpha}$ couplings differ at the C-terminus of each peptide at both 10 °C (Figure 6) and 37 °C (Figure S6 of the

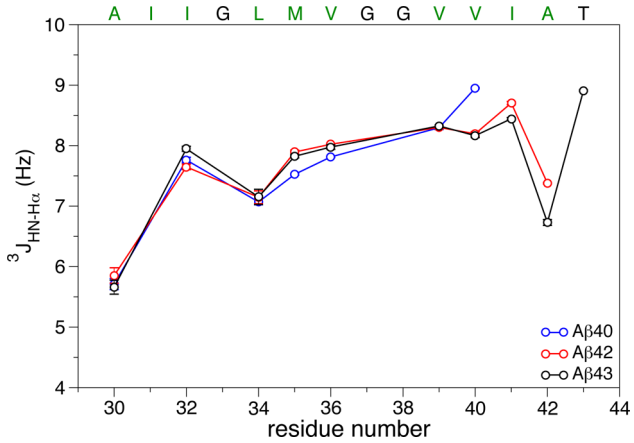

Figure 6. $^3J_{HN\text{-}H\alpha}$ couplings for residues A30 through the C-terminus of Aβ40 (blue), Aβ42 (red), and Aβ43 (black). Error bars denote the standard deviation.

Supporting Information). The near-maximal possible $^3J_{HN\text{-}H\alpha}$ value of T43 (8.9 Hz) demonstrates that the terminal residue of Aβ43 adopts a ϕ angle near −120° far more often than the terminal alanine of Aβ42 with a $^3J_{HN\text{-}H\alpha}$ value of 7.4 Hz. This difference is likely due to the increased extended conformation propensity due to branching at Cβ.[39] However, ^{13}Cα, ^{13}Cβ, ^{1}Hα, and ^{1}Hβ and chemical shifts for the C-termini of Aβ42 and Aβ43 from natural abundance ^{1}H−^{13}C HSQC spectra (Figure S7 of the Supporting Information) demonstrate no significant shift differences in resolvable nonterminal residues except a 0.2 ppm upfield Cα shift for I41, consistent with a slightly lower helical or higher extended/coil propensity based on refDB statistics for Ile.[40] Taken together, significant dynamical differences across the C-terminus and measurable differences in ^1H_N and ^{15}N chemical shifts without hallmarks of the formation of stable secondary structure (e.g., increased level of chemical shift dispersion and changes in Cα and Cβ chemical shifts, large differences in $^3J_{HN\text{-}H\alpha}$) suggest that addition of T43 changes the population of transiently formed structure in the C-terminal region of monomeric Aβ.

Structure and Dynamics in Protofibril-Bound States of Aβ43. Because our previous work demonstrated that the additional residues in Aβ42 led to motions in the protofibril-bound state slower than those of Aβ40, we used the same combination of ^{15}N ΔR_2 and DEST NMR to determine if the additional threonine in Aβ43 also demonstrated slowed C-terminal dynamics in the protofibril-bound state. By measurement of the difference between transverse relaxation rates, ^{15}N ΔR_2, in the presence of Aβ43 protofibrils (high concentration, 120 μM) and in a low-concentration reference sample without protofibrils (25 μM), a residue-by-residue picture of the interactions stabilizing binding of Aβ43 to protofibrils begins to emerge. In-phase ^{15}N R_2 values for 25 μM Aβ43 range from 1.60 ± 0.03 to 5.6 ± 0.2 s^{-1}, representing those expected for a peptide of this size under these conditions. For samples of 120 μM total Aβ43, where approximately 10% of the peptide remains monomeric, R_2 values are consistently higher, from 2.8

dx.doi.org/10.1021/bi500131a | Biochemistry 2014, 53, 3095−3105

± 0.1 to 8.0 ± 0.6 s^{-1}. It is important to note that the smooth variation in ΔR_2 from position to position observed here (Figure 7a) and the external field and nucleus (^{15}N vs $^{1}H_N$)

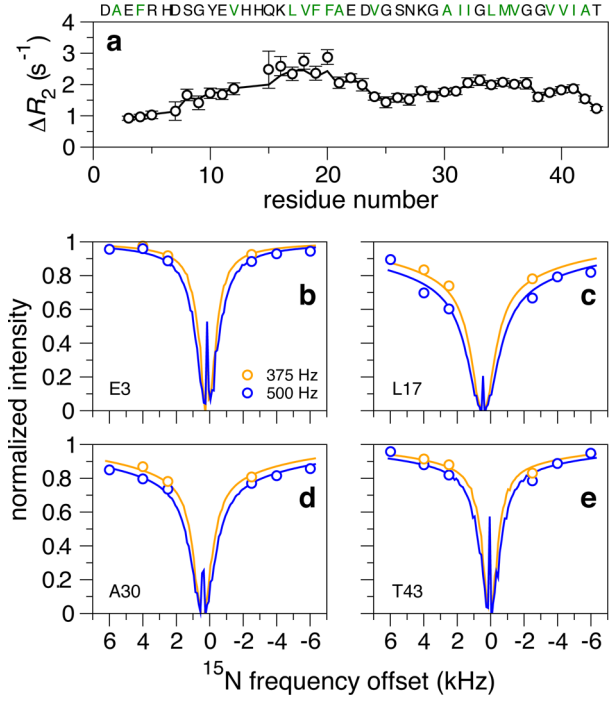

Figure 7. Protofibril-bound state of Aβ43 probed at atomic resolution by ^{15}N ΔR_2 and dark-state exchange saturation transfer (DEST) NMR spectroscopy. (a) The enhancements in ^{15}N transverse relaxation rates [^{15}N ΔR_2 (○)] of 120 μM Aβ43 compared to those of 25 μM samples arise due to interactions of the NMR visible monomeric peptide with the protofibrils. The best-fit ^{15}N ΔR_2 is illustrated with the solid black line. (b–e) ^{15}N DEST experiments. The normalized intensity of Aβ43 monomer resonances as a function of saturation at kilohertz offsets from the ^{15}N carrier frequency (119 ppm). Radiofrequency fields of 500 and 375 Hz at frequency offsets from 6 to −6 kHz were used to saturate the protofibrillar dark state with single-residue specificity, shown for residues E3, L17, A30, and T43. Lines indicate the calculated saturation profiles using the best-fit parameters for a ^{15}N spin in a model incorporating both tethered and direct contact states. Error bars denote the standard deviation.

independence we described previously for Aβ40 and Aβ42 under these conditions indicate that ΔR_2 does not arise from intermediate time scale chemical exchange broadening, but rather a lifetime broadening effect due to binding of the NMR visible monomer to the very high-molecular weight (>2 MDa) protofibril where transverse ^{15}N magnetization relaxes rapidly (faster than the rate of unbinding).[41] In the case of Aβ43, the maximal ΔR_2 of 2.9 ± 0.2 s^{-1} (Figure 7a) represents instead the apparent first-order association rate constant (k_{on}^{app}) for binding. This finding is similar to the previously reported values for Aβ40 (3.0 ± 0.2 s^{-1}) at 270 μM and Aβ42 (2.4 ± 0.2 s^{-1}) at 150 μM.[26]

Residue-by-residue behavior in the protofibril-bound state in exchange with the population of monomers of Aβ43 can be probed directly using DEST NMR. The experiment can be summarized as follows. Longitudinal ^{15}N magnetization prepared in the DEST experiment is efficiently saturated by weak, off-resonance, continuous wave pulses only in the slowly tumbling protofibrils; the monomer is largely unaffected. This saturation is then transferred to the pool of monomers when peptides unbind from the aggregates. The subsequent attenuation of the monomeric Aβ43 resonances is residue-specific (Figure 7b–e). The attenuation varies on the basis of the conformation and motions in the protofibrillar state, with greater attenuation observed for slower moving regions, revealing structural and dynamic details of the protofibril-bound state.

An atomically detailed model of the dynamic binding of Aβ peptides to protofibrils can be created by combining the results of DEST NMR and ΔR_2 experiments, as we have recently demonstrated for Aβ40 and Aβ42.[26] As was the case for Aβ40 and Aβ42, a two-state model with a single protofibril-bound state, where each residue has a unique fit parameter for R_2 in the bound state, cannot fit all the data simultaneously. However, the DEST and ΔR_2 data are consistent with a simple modification to the two-state model where each residue in the protofibril-bound state can be in direct contact with the aggregate surface or tethered to the surface by the binding of residues further down the chain (Figure 8a). In this model, each residue experiences the same transverse relaxation rate when in direct contact with the surface, $R_2^{contact}$, reflecting the common, slow motions of the protofibril, and two residue-specific properties: the ratio of the time spent in direct-contact states versus states tethered to the surface via the direct interactions of other residues in the same chain, K_3, and the average transverse relaxation rate when tethered, ^{15}N $R_2^{tethered}$. This model adds the fewest number of parameters to a two-state model that allows a good fit to the experimental data.[26] The first-order rate constant describing the binding of the monomer to the protofibril, k_{on}^{app}, is set to 3 s^{-1}, the maximal value of ΔR_2. Because the low equilibrium monomer concentration (12 μM) and accompanying low signal-to-noise ratio limited the number of high-quality data points that can be measured in a 5 day DEST experiment compared to that previously measured for Aβ40 and Aβ42, the global kinetic parameters relating the binding and unbinding of Aβ from the protofibrils at equilibrium could not be uniquely determined from the DEST and ΔR_2 data. $R_2^{contact}$ is consistent with a single, residue-independent value ranging from 10000 to 30000 s^{-1} and was set to 19000 s^{-1} to match the values previously determined for Aβ40 and Aβ42.[26] The population of transiently protofibril-bound monomer, p_B, is consistent with values from 2 to 10%. Choosing a value of 4%, the same as that for Aβ42 and similar to that for Aβ40 (6%), in combination with an $R_2^{contact}$ of 19000 s^{-1} results in N-terminal values of residue-specific $R_2^{tethered}$ similar to those for both Aβ40 and Aβ42, and hence this choice was made for further analysis. Although the values of $R_2^{contact}$ and p_B affect the quantitative values of the residue-specific parameters, the interpretation of the data is independent of the chosen values (see Figure S8 of the Supporting Information).

The simple extension to the two-state model captures an atomic level picture of the dynamic ensemble of protofibril-bound structures in two residue-specific parameters, K_3 and $R_2^{tethered}$. K_3, measuring the ratio of direct contact to tethered states at any given residue, for Aβ43 is highest across residues 17–21 and residues 30–36 (Figure 8b), which comprise the central and C-terminal hydrophobic regions of the peptide, respectively, indicating that these residues are most likely to bind directly to the protofibril surface. In contrast, lower values of K_3 are found at the hydrophilic regions at the N-terminus and the region connecting the hydrophobic patches. This pattern is similar to that found for Aβ40 and Aβ42. The average

dx.doi.org/10.1021/bi500131a | Biochemistry 2014, 53, 3095–3105

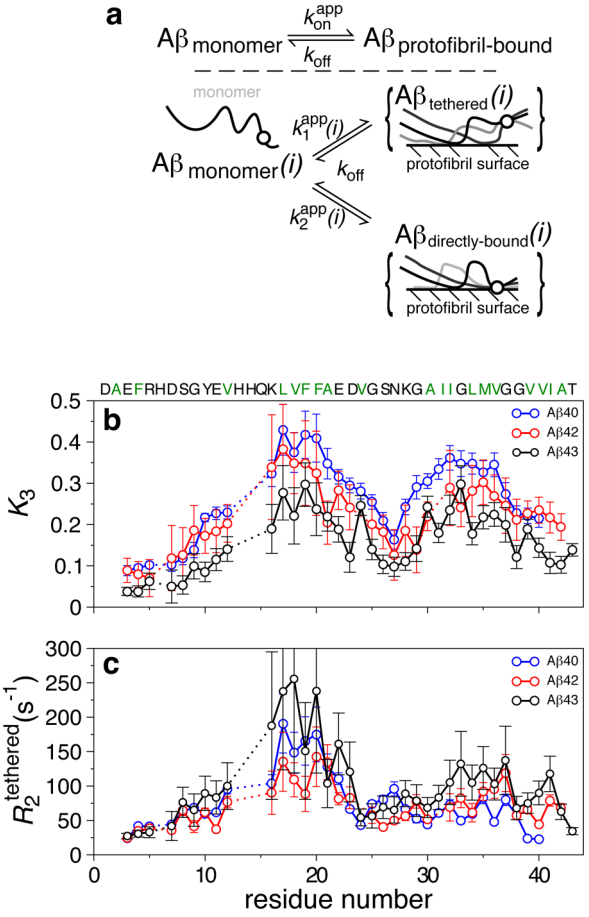

Figure 8. Binding model and local parameters describing Aβ43 monomer−protofibril interactions. (a) The dynamic binding of Aβ43 to protofibrils can be described by a model incorporating two different ensembles of states for each residue: in direct contact with the surface or tethered via the binding of other residues. (b) Residue-specific equilibrium constant (K_3) values for Aβ40 (blue), Aβ42 (red), and Aβ43 (black) describing the relative ratio of direct contact and tethered states for each residue. (c) Residue-specific ^{15}N $R_2^{tethered}$ values for Aβ40 (blue), Aβ42 (red), and Aβ43 (black) describing the average structure and motions of each residue when it is tethered to protofibrils by the binding of other residues in the same chain. Error bars denote the standard deviation. Values presented for Aβ40 and Aβ42 were taken from ref 26.

value of K_3 for Aβ43 for the fit parameters described above is lower than that of Aβ42, which is lower than that of Aβ40. This inverse dependence on Aβ length is likely a result of an increasing level of competition between additional protofibril-binding sites on the Aβ peptide with an increasing length. Unlike both Aβ42 and Aβ40 where the value of K_3 falls at the C-terminus, the value of K_3 rises at T43, indicating that the terminal threonine of Aβ43 plays a role in directly mediating contact with protofibrillar aggregates.

The residue-specific values of $R_2^{tethered}$ provide a quantitative measure of the average motions of each residue of Aβ43 when it is tethered to the protofibril surface (Figure 8c). Larger values of $R_2^{tethered}$ correspond to slower motions, most likely due to shorter tethering lengths. As previously observed for Aβ40 and Aβ42, $R_2^{tethered}$ values for Aβ43 are lowest in the hydrophilic N-terminal region, suggesting they are most often far from the aggregate surface when other residues mediate direct interaction. $R_2^{tethered}$ values are higher in hydrophobic regions and closely match those of Aβ42, showing significantly slower motions than Aβ40 in the C-terminal hydrophobic region. Taken together, these data suggest protofibril-bound states of Aβ43 are structurally and dynamically more similar to those of Aβ42 than those of Aβ40, with additional interactions in the protofibril-bound state mediated directly by T43.

DISCUSSION

Recent evidence points to the potential of Aβ peptides other than the most common Aβ40 and Aβ42 to seed toxic aggregates in AD.[32] Among these low-population species, Aβ43 is of particular interest because its aggregation is a hallmark of sporadic AD,[30] the most common form of AD, whose molecular origins are currently unknown.

Here, we characterized the changes in the aggregation and structural properties of the Aβ peptide introduced by the addition of a single C-terminal threonine residue to form Aβ43. This terminal extension alters the structure and dynamics of both the monomeric state and the resulting protofibrillar aggregates. In the monomeric state, slower motions that cannot be explained simply by a longer peptide are evident across the C-terminus of Aβ43 relative to Aβ42 (Figure 4), supporting the hypothesis of Wang and co-workers that slower motions in the monomeric state of Aβ are correlated with a higher aggregation propensity.[12] These dynamical differences are accompanied by differences in chemical shifts (Figure 5 and Figure S7 of the Supporting Information), suggesting that slower motions in Aβ43 can be attributed to a distinct structural ensemble compared to that of Aβ42. Although the structural ensemble is difficult to determine directly because of the extremely low equilibrium concentration (12 μM), Aβ43 chemical shifts are consistent with a highly disordered protein as is observed for Aβ40 and Aβ42,[13,42] though small chemical shift differences across the C-terminus likely arise from changes in transiently populated structures (e.g., hydrogen-bonded turns). Differences in the monomeric state are mirrored in the aggregation of Aβ43, which more rapidly forms protofibrils and has a critical aggregation concentration much lower than those of Aβ42 and Aβ40 (Figure 2). In the protofibril-bound state, the slow dynamics of the C-terminal residues when they are tethered and the partitioning into tethered and directly bound states of Aβ43 more closely resemble those of Aβ42 than those of Aβ40, demonstrating a correlation between the aggregation behavior and the dynamics in the protofibril-bound state. In addition, the C-terminus of Aβ43 is involved in direct contact with the aggregates more often than the adjacent residues, unlike at the termini of Aβ40 and Aβ42. Stabilizing contacts between the C-terminal ends of Aβ peptides at the core of transient oligomeric aggregates are critical for overcoming the critical nucleus for formation of partially ordered stable aggregates including protofibrils.[43] Hence, the direct contacts formed by the C-terminal threonine may provide an explanation for the protofibril formation of Aβ43 being much more rapid than that of Aβ42. In summary, these results support the hypothesis that small but significant differences in the monomeric and protofibrillar structure and dynamics of Aβ43 result in an increased aggregation propensity, providing an explanation for the observed enhanced toxicity of Aβ43 and a possible mechanism for its suspected role in sporadic AD.

The correlation between C-terminal Aβ length and aggregation propensity has been studied extensively, primarily comparing the most common species, Aβ40 and Aβ42. Lansbury and co-workers demonstrated that C-terminal

dx.doi.org/10.1021/bi500131a | Biochemistry 2014, 53, 3095−3105

fragments of long Aβ species, Aβ26−42 and Aβ26−43, showed aggregation much more rapid than that of Aβ26−40 but could not resolve a difference between these species.[9] Similarly, Vandersteen et al. demonstrate that Aβ43 and Aβ42 both aggregate rapidly, without a distinct lag phase in fibril formation monitored by thioflavin T fluorescence, but could not quantitatively distinguish the aggregation rates of Aβ42 from Aβ43.[32] We have shown that Aβ43 does dramatically increase the rate and extent of protofibril aggregation relative to those of Aβ42. Our results demonstrate that this higher aggregation propensity is associated with slower motions in both the monomeric and protofibril-bound states. Furthermore, our data attribute this difference in dynamics to small but critical structural changes in the C-terminal structural ensemble, similar to the significant structural differences observed for Aβ42 due to the two additional residues present relative to Aβ40.[44] Although our results probe the structure, motions, and aggregation of Aβ43 at atomic resolution, future studies using molecular simulation may shed light on the specific contacts stabilized by T43 in the monomeric and protofibril-bound state that are difficult to exhaustively characterize using experiments alone. The differences between the chemical shifts, R_2, and DEST parameters of Aβ43 relative to those of Aβ42 reported here will serve as important residue-specific observables for direct validation of both the structure and dynamics of simulated ensembles, as we have previously demonstrated for shorter Aβ peptides.[35,45]

Although high-resolution NMR experiments offer the ability to study the structure and aggregation of Aβ peptides with atomistic precision, the conditions used here are entirely *in vitro* under a single set of conditions, and the behavior under other conditions as well as *in vivo* may be different. One important difference between these experimental conditions commonly used for *in vitro* studies and the native environment is the concentration of Aβ; while we used concentrations of >10 μM, Aβ peptides are typically present at concentrations of ∼25 nM. However, the native environment is not homogeneous, and recent work suggests that aggregation is initiated within endosomes that concentrate Aβ to the micromolar range, leading to subsequent seeding of extracellular amyloid formation.[46] Hence, the concentrations used for this work potentially correspond to the effective conditions *in vivo*; the critical concentration in the low micromolar range and more rapid aggregation of Aβ43, compared to that of Aβ42, lead us to hypothesize that Aβ43 is able to nucleate toxic aggregates in endocytic compartments much more frequently than shorter Aβ species. Therefore, we propose a model in which Aβ43 aggregates either with itself or with other highly aggregation-prone Aβ variants to seed subsequent Aβ42 aggregation. The biochemical changes that lead to even a small increase in the level of production of Aβ43, because of impaired γ-secretase activity along the pathway to form Aβ40, may be a critical trigger for AD. Additionally, therapeutic strategies attempting to clear Aβ using either active (Aβ immunization) or passive (administration of Aβ-binding antibodies) targeting specifically Aβ43 should be investigated. For example, in the mouse model of Saito et al. where Aβ43 is overproduced because of a mutation, the ability of an Aβ43-specific immunotherapy to prevent both plaque formation and the observed neurological deficits could be tested. Further experiments to test the hypothesis that Aβ43 recruits Aβ42 aggregation *in vitro* by determining the aggregation rates and atomic resolution mechanism of co-aggregation in mixtures of Aβ peptides containing Aβ43 are ongoing in the laboratory.

■ ASSOCIATED CONTENT

Ⓢ Supporting Information

The 37 °C aggregation time course and TEM imaging; overlay of ^{15}N R_2 values for Aβ43 measured at 15 and 25 μM and for Aβ43 and Aβ42 measured under denaturing conditions; overlay of chemical shift differences between Aβ43 and Aβ42 observed under native conditions (10 and 37 °C) and denaturing conditions; correlation plot of $^3J_{HN\text{-}H\alpha}$ values measured by line-shape analysis and reported previously; overlay of $^3J_{HN\text{-}H\alpha}$ values at 10 and 37 °C; Cα region of $^1H-^{13}C$ HSQC of Aβ42 and Aβ43; and comparison of the effect of p_B values on best-fit residue-specific parameters. This material is available free of charge via the Internet at http://pubs.acs.org.

■ AUTHOR INFORMATION

Corresponding Author

*Address: 70 Ship St., Box G-E, Providence, RI 02912. E-mail: Nicolas_Fawzi@brown.edu. Phone: (401) 863-5232.

Funding

Research reported in this publication was supported in part by a pilot project award to N.L.F. as part of an Institutional Development Award (IDeA) from the National Institute of General Medical Sciences of the National Institutes of Health via Grant 5 P20 GM103430-13. A.E.C. was a predoctoral trainee supported in part by Grant T32-GM07601. This research is based in part upon work conducted using the Rhode Island NSF/EPSCoR Proteomics Shared Resource Facility, which is supported in part by National Science Foundation EPSCoR Grant 1004057, National Institutes of Health Grant 1S10RR020923, a Rhode Island Science and Technology Advisory Council grant, and the Division of Biology and Medicine, Brown University. This research is based in part on data obtained at the Brown University Structural Biology Core Facility, which is supported by the Division of Biology and Medicine, Brown University.

Notes

The authors declare no competing financial interest.

■ ACKNOWLEDGMENTS

We thank Michael "Sparky" Clarkson for technical assistance and helpful conversations, Art Salomon for use of lyophilization equipment, Rute Silva for wet laboratory assistance, Jinfa Ying and David Libich for helpful discussions regarding scalar coupling and chemical shift measurements, and Geoff Williams and the Leduc Bioimaging Facility at Brown University for assistance with the transmission electron microscopy described in this study. We also thank the Center for Computation and Visualization at Brown University for providing the computational resources required for running the DESTfit software. We thank Chunyu Wang and David Rosenman for providing their published experimental $^3J_{HN\text{-}H\alpha}$ data.

■ ABBREVIATIONS

NMR, nuclear magnetic resonance; AD, Alzheimer's disease; FAD, familial Alzheimer's disease; Aβ, amyloid β; DEST, dark-state exchange saturation transfer; HSQC, heteronuclear single-quantum coherence; TEM, transmission electron microscopy; R_1, longitudinal relaxation rate constant; R_2, transverse relaxation rate constant; CPMG, Carr−Purcell−Meiboom−

Gill; NOE, nuclear Overhauser effect; $^3J_{HN\text{-}H\alpha}$, three-bond (HN−Hα) scalar coupling constant.

REFERENCES

(1) Hardy, J., and Selkoe, D. J. (2002) The amyloid hypothesis of Alzheimer's disease: Progress and problems on the road to therapeutics. *Science 297*, 353−356.

(2) Dickson, D. W., Crystal, H. A., Bevona, C., Honer, W., Vincent, I., and Davies, P. (1995) Correlations of synaptic and pathological markers with cognition of the elderly. *Neurobiol. Aging 16*, 285−298 , 298−304 (discussion).

(3) McLean, C. A., Cherny, R. A., Fraser, F. W., Fuller, S. J., Smith, M. J., Beyreuther, K., Bush, A. I., and Masters, C. L. (1999) Soluble pool of Aβ amyloid as a determinant of severity of neurodegeneration in Alzheimer's disease. *Ann. Neurol. 46*, 860−866.

(4) Walsh, D. M., Hartley, D. M., Kusumoto, Y., Fezoui, Y., Condron, M. M., Lomakin, A., Benedek, G. B., Selkoe, D. J., and Teplow, D. B. (1999) Amyloid β-protein fibrillogenesis. Structure and biological activity of protofibrillar intermediates. *J. Biol. Chem. 274*, 25945−25952.

(5) Lue, L. F., Kuo, Y. M., Roher, A. E., Brachova, L., Shen, Y., Sue, L., Beach, T., Kurth, J. H., Rydel, R. E., and Rogers, J. (1999) Soluble amyloid β peptide concentration as a predictor of synaptic change in Alzheimer's disease. *Am. J. Pathol. 155*, 853−862.

(6) Benilova, I., Karran, E., and De Strooper, B. (2012) The toxic Aβ oligomer and Alzheimer's disease: An emperor in need of clothes. *Nat. Neurosci. 15*, 349−357.

(7) Zhao, G., Mao, G., Tan, J., Dong, Y., Cui, M. Z., Kim, S. H., and Xu, X. (2004) Identification of a new presenilin-dependent ζ-cleavage site within the transmembrane domain of amyloid precursor protein. *J. Biol. Chem. 279*, 50647−50650.

(8) Steiner, H., Fluhrer, R., and Haass, C. (2008) Intramembrane proteolysis by γ-secretase. *J. Biol. Chem. 283*, 29627−29631.

(9) Jarrett, J. T., Berger, E. P., and Lansbury, P. T., Jr. (1993) The carboxy terminus of the β amyloid protein is critical for the seeding of amyloid formation: Implications for the pathogenesis of Alzheimer's disease. *Biochemistry 32*, 4693−4697.

(10) Borchelt, D. R., Thinakaran, G., Eckman, C. B., Lee, M. K., Davenport, F., Ratovitsky, T., Prada, C. M., Kim, G., Seekins, S., Yager, D., Slunt, H. H., Wang, R., Seeger, M., Levey, A. I., Gandy, S. E., Copeland, N. G., Jenkins, N. A., Price, D. L., Younkin, S. G., and Sisodia, S. S. (1996) Familial Alzheimer's disease-linked presenilin 1 variants elevate Aβ1−42/1−40 ratio in vitro and in vivo. *Neuron 17*, 1005−1013.

(11) Yan, Y., Liu, J., McCallum, S. A., Yang, D., and Wang, C. (2007) Methyl dynamics of the amyloid-β peptides Aβ40 and Aβ42. *Biochem. Biophys. Res. Commun. 362*, 410−414.

(12) Yan, Y., and Wang, C. (2006) Aβ42 is more rigid than Aβ40 at the C terminus: Implications for Aβ aggregation and toxicity. *J. Mol. Biol. 364*, 853−862.

(13) Riek, R., Guntert, P., Dobeli, H., Wipf, B., and Wuthrich, K. (2001) NMR studies in aqueous solution fail to identify significant conformational differences between the monomeric forms of two Alzheimer peptides with widely different plaque-competence, Aβ(1−40)(ox) and Aβ(1−42)(ox). *Eur. J. Biochem. 268*, 5930−5936.

(14) Lu, J. X., Qiang, W., Yau, W. M., Schwieters, C. D., Meredith, S. C., and Tycko, R. (2013) Molecular structure of β-amyloid fibrils in Alzheimer's disease brain tissue. *Cell 154*, 1257−1268.

(15) Luhrs, T., Ritter, C., Adrian, M., Riek-Loher, D., Bohrmann, B., Dobeli, H., Schubert, D., and Riek, R. (2005) 3D structure of Alzheimer's amyloid-β(1−42) fibrils. *Proc. Natl. Acad. Sci. U.S.A. 102*, 17342−17347.

(16) Zhang, R., Hu, X., Khant, H., Ludtke, S. J., Chiu, W., Schmid, M. F., Frieden, C., and Lee, J. M. (2009) Interprotofilament interactions between Alzheimer's Aβ1−42 peptides in amyloid fibrils revealed by cryoEM. *Proc. Natl. Acad. Sci. U.S.A. 106*, 4653−4658.

(17) Abelein, A., Kaspersen, J. D., Nielsen, S. B., Jensen, G. V., Christiansen, G., Pedersen, J. S., Danielsson, J., Otzen, D. E., and Graslund, A. (2013) Formation of dynamic soluble surfactant-induced amyloid β peptide aggregation intermediates. *J. Biol. Chem. 288*, 23518−23528.

(18) Ladiwala, A. R., Litt, J., Kane, R. S., Aucoin, D. S., Smith, S. O., Ranjan, S., Davis, J., Van Nostrand, W. E., and Tessier, P. M. (2012) Conformational differences between two amyloid β oligomers of similar size and dissimilar toxicity. *J. Biol. Chem. 287*, 24765−24773.

(19) Ahmed, M., Davis, J., Aucoin, D., Sato, T., Ahuja, S., Aimoto, S., Elliott, J. I., Van Nostrand, W. E., and Smith, S. O. (2010) Structural conversion of neurotoxic amyloid-β(1−42) oligomers to fibrils. *Nat. Struct. Mol. Biol. 17*, 561−567.

(20) Carulla, N., Zhou, M., Arimon, M., Gairi, M., Giralt, E., Robinson, C. V., and Dobson, C. M. (2009) Experimental characterization of disordered and ordered aggregates populated during the process of amyloid fibril formation. *Proc. Natl. Acad. Sci. U.S.A. 106*, 7828−7833.

(21) Scheidt, H. A., Morgado, I., and Huster, D. (2012) Solid-state NMR reveals a close structural relationship between amyloid-β protofibrils and oligomers. *J. Biol. Chem. 287*, 22822−22826.

(22) Bertini, I., Gallo, G., Korsak, M., Luchinat, C., Mao, J., and Ravera, E. (2013) Formation kinetics and structural features of β-amyloid aggregates by sedimented solute NMR. *ChemBioChem 14*, 1891−1897.

(23) Narayanan, S., and Reif, B. (2005) Characterization of chemical exchange between soluble and aggregated states of β-amyloid by solution-state NMR upon variation of salt conditions. *Biochemistry 44*, 1444−1452.

(24) Dasari, M., Espargaro, A., Sabate, R., Lopez del Amo, J. M., Fink, U., Grelle, G., Bieschke, J., Ventura, S., and Reif, B. (2011) Bacterial inclusion bodies of Alzheimer's disease β-amyloid peptides can be employed to study native-like aggregation intermediate states. *ChemBioChem 12*, 407−423.

(25) Krishnamoorthy, J., Brender, J. R., Vivekanandan, S., Jahr, N., and Ramamoorthy, A. (2012) Side-chain dynamics reveals transient association of Aβ(1−40) monomers with amyloid fibers. *J. Phys. Chem. B 116*, 13618−13623.

(26) Fawzi, N. L., Ying, J., Ghirlando, R., Torchia, D. A., and Clore, G. M. (2011) Atomic-resolution dynamics on the surface of amyloid-β protofibrils probed by solution NMR. *Nature 480*, 268−272.

(27) Jawhar, S., Wirths, O., and Bayer, T. A. (2011) Pyroglutamate amyloid-β (Aβ): A hatchet man in Alzheimer disease. *J. Biol. Chem. 286*, 38825−38832.

(28) Saito, T., Suemoto, T., Brouwers, N., Sleegers, K., Funamoto, S., Mihira, N., Matsuba, Y., Yamada, K., Nilsson, P., Takano, J., Nishimura, M., Iwata, N., Van Broeckhoven, C., Ihara, Y., and Saido, T. C. (2011) Potent amyloidogenicity and pathogenicity of Aβ43. *Nat. Neurosci. 14*, 1023−1032.

(29) Welander, H., Franberg, J., Graff, C., Sundstrom, E., Winblad, B., and Tjernberg, L. O. (2009) Aβ43 is more frequent than Aβ40 in amyloid plaque cores from Alzheimer disease brains. *J. Neurochem. 110*, 697−706.

(30) Sandebring, A., Welander, H., Winblad, B., Graff, C., and Tjernberg, L. O. (2013) The pathogenic Aβ43 is enriched in familial and sporadic Alzheimer disease. *PLoS One 8*, e55847.

(31) Zou, K., Liu, J., Watanabe, A., Hiraga, S., Liu, S., Tanabe, C., Maeda, T., Terayama, Y., Takahashi, S., Michikawa, M., and Komano, H. (2013) Aβ43 is the earliest-depositing Aβ species in APP transgenic mouse brain and is converted to Aβ41 by two active domains of ACE. *Am. J. Pathol. 182*, 2322−2331.

(32) Vandersteen, A., Masman, M. F., De Baets, G., Jonckheere, W., van der Werf, K., Marrink, S. J., Rozenski, J., Benilova, I., De Strooper, B., Subramaniam, V., Schymkowitz, J., Rousseau, F., and Broersen, K. (2012) Molecular plasticity regulates oligomerization and cytotoxicity of the multipeptide-length amyloid-β peptide pool. *J. Biol. Chem. 287*, 36732−36743.

(33) Delaglio, F., Grzesiek, S., Vuister, G. W., Zhu, G., Pfeifer, J., and Bax, A. (1995) NMRPipe: A multidimensional spectral processing system based on UNIX pipes. *J. Biomol. NMR 6*, 277−293.

(34) Fawzi, N. L., Ying, J., Torchia, D. A., and Clore, G. M. (2012) Probing exchange kinetics and atomic resolution dynamics in high-

molecular-weight complexes using dark-state exchange saturation transfer NMR spectroscopy. *Nat. Protoc. 7*, 1523−1533.
(35) Fawzi, N. L., Phillips, A. H., Ruscio, J. Z., Doucleff, M., Wemmer, D. E., and Head-Gordon, T. (2008) Structure and dynamics of the Aβ(21−30) peptide from the interplay of NMR experiments and molecular simulations. *J. Am. Chem. Soc. 130*, 6145−6158.
(36) Kragelj, J., Ozenne, V., Blackledge, M., and Jensen, M. R. (2013) Conformational propensities of intrinsically disordered proteins from NMR chemical shifts. *ChemPhysChem 14*, 3034−3045.
(37) Maltsev, A. S., Ying, J., and Bax, A. (2012) Impact of N-terminal acetylation of α-synuclein on its random coil and lipid binding properties. *Biochemistry 51*, 5004−5013.
(38) Rosenman, D. J., Connors, C. R., Chen, W., Wang, C., and Garcia, A. E. (2013) Aβ monomers transiently sample oligomer and fibril-like configurations: Ensemble characterization using a combined MD/NMR approach. *J. Mol. Biol. 425*, 3338−3359.
(39) Minor, D. L., Jr., and Kim, P. S. (1994) Measurement of the β-sheet-forming propensities of amino acids. *Nature 367*, 660−663.
(40) Zhang, H., Neal, S., and Wishart, D. S. (2003) RefDB: A database of uniformly referenced protein chemical shifts. *J. Biomol. NMR 25*, 173−195.
(41) Fawzi, N. L., Ying, J., Torchia, D. A., and Clore, G. M. (2010) Kinetics of amyloid β monomer-to-oligomer exchange by NMR relaxation. *J. Am. Chem. Soc. 132*, 9948−9951.
(42) Hou, L., Shao, H., Zhang, Y., Li, H., Menon, N. K., Neuhaus, E. B., Brewer, J. M., Byeon, I. J., Ray, D. G., Vitek, M. P., Iwashita, T., Makula, R. A., Przybyla, A. B., and Zagorski, M. G. (2004) Solution NMR studies of the Aβ(1−40) and Aβ(1−42) peptides establish that the Met35 oxidation state affects the mechanism of amyloid formation. *J. Am. Chem. Soc. 126*, 1992−2005.
(43) Fawzi, N. L., Okabe, Y., Yap, E. H., and Head-Gordon, T. (2007) Determining the critical nucleus and mechanism of fibril elongation of the Alzheimer's Aβ(1−40) peptide. *J. Mol. Biol. 365*, 535−550.
(44) Ball, K. A., Phillips, A. H., Wemmer, D. E., and Head-Gordon, T. (2013) Differences in β-strand populations of monomeric Aβ40 and Aβ42. *Biophys. J. 104*, 2714−2724.
(45) Ball, K. A., Phillips, A. H., Nerenberg, P. S., Fawzi, N. L., Wemmer, D. E., and Head-Gordon, T. (2011) Homogeneous and heterogeneous tertiary structure ensembles of amyloid-β peptides. *Biochemistry 50*, 7612−7628.
(46) Hu, X., Crick, S. L., Bu, G., Frieden, C., Pappu, R. V., and Lee, J. M. (2009) Amyloid seeds formed by cellular uptake, concentration, and aggregation of the amyloid-β peptide. *Proc. Natl. Acad. Sci. U.S.A. 106*, 20324−20329.